Non-Extensive Statistical Analysis of Seismicity in the West Coastline of Mexico

Elsa Leticia Flores-Márquez ---X * , Alejandro Ramírez-Rojas , Leonardo Di G. Sigalotti

Posted Date: 1 May 2024

doi: 10.20944/preprints202405.0076.v1

Keywords: gutenberg-richter law; tsallis entropy; non-extensive statistics; earthquakes; mexican seismicity; plate tectonics

 doi:10.20944/preprints202405.0076.v1

Article

Non-Extensive Statistical Analysis of Seismicity in the West Coastline of Mexico

Elsa Leticia Flores-Márquez [1,*], Alejandro Ramírez-Rojas [2] and Leonardo Di G. Sigalotti [2]

[1] Instituto de Geofísica, Universidad Nacional Autónoma de México; Circuito de la Investigación Científica, Ciudad Universitaria, Alcaldía Coyoacán, Mexico City 04510, Mexico; leticia@igeofisica.unam.mx
[2] Departamento de Ciencias Básicas, Universidad Autónoma Metropolitana-Azcapotzalco, Av. San Pablo 420, Colonia Nueva el Rosario, Alcaldía Azcapotzalco, Mexico City 02128, Mexico; arr@azc.uam.mx; leonardo.sigalotti@gmail.com
* Correspondence: leticia@igeofisica.unam.mx; Tel.: +52-5537-1918-29 (F.L.)
‡ These authors contributed equally to this work.

Abstract: Mexico is a well-known seismically active country, which is primarily affected by several tectonic plate interactions along the southern Pacific coastline and by active structures in the Gulf of Baja California. In this paper we investigate this seismicity in the context of a non-extensive statistical approach based on Tsallis entropy. The analysis is performed using data from the corrected Mexican seismic catalogue provided by the National Seismic Service, spanning a period from January 2000 to October 2023. The Gutenberg-Richter law fitting to the earthquake sub-catalogues for all six regions studied indicates magnitudes of completeness between 3.30 and 3.76. All six regions display values of the entropic index in the range $1.52 \lesssim q \lesssim 1.61$, which are lower than the previously estimated range $1.54 \lesssim q \lesssim 1.70$ using catalogue data from 1988 to 2010. The cause of this discrepancy is certainly due to the use of modern recording devices, which are sensitive enough to detect a larger number of low-magnitude events compared to older instrumentation.

Keywords: gutenberg-richter law; tsallis entropy; non-extensive statistics; earthquakes; mexican seismicity; plate tectonics

1. Introduction

Non-extensive statistical mechanics (NESM) based on Tsallis formalism [1–3] represents a robust theoretical framework for the description and interpretation of non-equilibrium complex systems, including real seismicity, faulting and plate tectonics with a special focus on the mechanism(s) of earthquake generation. Since earthquakes are often catastrophic events, understanding their physics is a mandatory aspect of research in seismology and of high priority in many seismic countries.

In particular, Tsallis' NESM, or q-statistics, is a generalization of the Boltzmann-Gibbs (BG) statistics with additive entropy into a NESM with a non-additive entropy function that allows the description of physical processes involving long-range interactions, long-term memories and multifractal properties [4]. In contrast to GB thermodynamics, a non-additive entropy was indeed necessary to account for correlations between different elements of the system at all length scales. Such correlations lead to broad distributions with a power-law asymptotic behavior. For a detailed description of Tsallis' theory the interested reader is referred to papers and books in Refs.[2,3,5–7]. Since its development, NESM has been applied to the analysis of the macroscopic properties of earthquakes to both regional [8,9] and global scales [10]. In a seminal paper, Sotolongo-Costa and Posadas [11] developed a model for the physical mechanism of earthquake triggering – the so-called fragment-asperity model, based on the interaction between the fragments, generated by the local breaking of the tectonic plates and the asperity of the fault planes. Since then, a growing number of papers dealing with the analysis of seismicity, plate tectonics and precursory electromagnetic anomalies in different regions around the world have been devoted to demonstrate the consistency between NESM and observations. The Sotolongo-Costas and Posadas' [11] model for earthquake magnitudes was extended by Silva et al. [12] to include a relationship between the fragment size and the earthquake energy, which appears to be more consistent with the standard theory of seismic moment [13]. This improved formulation leads to a different earthquake magnitude distribution compared to Sotolongo-Costas and Posadas' model

 doi:10.20944/preprints202405.0076.v1

and it was found to fit equally well the magnitude distribution of several regional seismicities and local seismic zones around the world [14–23].

Mexico's seismicity is due to the fact that the country lies on the eastern rim of the Ring of Fire, where a large number of seismic events and volcanic eruptions occur in the basin of the Pacific Ocean. The country is particularly affected by the interaction between the Cocos Plate and the North American Plate. Such tectonic plate interactions are responsible for the fragmentation of the Earth's crust, which is the likely mechanism for triggering earthquakes. In particular, the seismicity of Mexico has been previously studied by a number of authors along the past four decades [19,24–35]. A natural time analysis of six tectonic zones in the Mexican Pacific coast revealed that extreme events could be expected in the Chiapas region [34]. Most recent analyses of the Mexican seismicity are therefore related with the deadly M8.2 earthquake [34,35], which was one of the largest Mexican seismic events. In this case, a precursory behavior three months before the occurrence of the M8.2 earthquake in Chiapas was identified using natural time [35], which was related with fluctuations of the entropy change under time reversal and an abrupt simultaneous increase of the Tsallis entropic index q [34]. In particular, a non-extensive analysis of the seismicity in Mexico based on Tsallis' q-statistics between 1988 and 2010 along the South Pacific coast, including the regions of Jalisco, Michoacán, Guerrero and Oaxaca, has been performed by Valverde-Esparza et al. [19]. These four regions are characterized by different subduction patterns and therefore by different tectonic regimes. They obtained q-values well in the range of those derived for other regions reported in the literature. For example, for the Jalisco region their analysis yielded $q = 1.7020$ against $q = 1.6845$, 1.6635 and 1.6370 for the Michoacán, Oaxaca and Guerrero regions, respectively. Since lower values of q indicate more stability, it was concluded that the subduction zone is more unstable in the northwestern coastline (Jalisco) than in the southeastern part (Guerrero and Oaxaca). These results are indicative of a possible correlation between the seismicity pattern associated with the inclination angle of each subduction zone and the value of the non-extensive parameter q.

In this paper the frequency-magnitude distribution of earthquakes along the entire Pacific coast of Mexico from the Gulf of Baja California to Chiapas is investigated in the framework of the classical Gutenberg-Richter (GR) relation and the non-extensive model for earthquakes revisited by Silva et al. [12]. The investigated seismicity includes six tectonic zones and the period analyzed spans from January 1, 2000 to October 13, 2023 as referred in the corrected Mexican seismic catalogue provided by the National Seismic Service (http://www.ssn.unam.mx). This paper is organized as follows. Section 2 is devoted to a brief description of NESP based on Tsallis entropy along with Silva et al.'s [12] non-extensive model for the earthquake energy distribution function and cumulative number of earthquakes. The tectonic setting is briefly described in Section 3, while the dataset description and analysis procedure are discussed in Section 4. Section 5 describes the results obtained and Section 6 summarizes the relevant conclusions.

2. Non-Extensive Statistical Mechanics

2.1. Non-Additive Tsallis Entropy and Probability Distribution

The integral formulation of the non-additive Tsallis entropy, S_q, for a continuous variable $\sigma \in \mathbb{R}$ can be written as [4]

$$S_q(\sigma) = \frac{k_B}{1-q}\left[1 - \int_0^\infty p^q(\sigma)d\sigma\right], \tag{1}$$

where k_B is the Boltzmann constant, $q \in \mathbb{R}$ is the non-extensive index (or parameter), σ stands for the characteristic surface of a fragment as in the Sotolongo-Costa and Posadas' [11] model and $p(\sigma) \in [0,1]$ is the probability of finding a fragment of surface σ. In the limit $q \to 1$, Equation (1) takes the form of the BG entropy of classical thermodynamics. Hereafter k_B is set to unity for simplicity. Maximization

 doi:10.20944/preprints202405.0076.v1

of the Tsallis entropy is required to determine $p(\sigma)$. A standard method relies on the maximization of the entropy functional [2]

$$\delta f_q(p, \lambda_0, \lambda_1) = \delta \left[S_q + \lambda_0 \int_0^\infty p(\sigma) d\sigma - \lambda_1 \langle \sigma \rangle_q \right] = 0, \tag{2}$$

under the two constraints [2,36]:

$$\int_0^\infty p(\sigma) d\sigma = 1, \tag{3}$$

and

$$\langle \sigma \rangle_q = \int_0^\infty \sigma \mathcal{P}_q(\sigma) d\sigma, \tag{4}$$

where λ_0 and λ_1 are the Lagrange multipliers, $\langle \sigma \rangle_q$ is the generalized q-expectation value defined in terms of the escort probability [36]

$$\mathcal{P}_q(\sigma) = p^q(\sigma) \left[\int_0^\infty p^q(\sigma) d\sigma \right]^{-1}, \tag{5}$$

with

$$\int_0^\infty \mathcal{P}_q(\sigma) d\sigma = 1. \tag{6}$$

Application of Equation (2) along with the constraints (3) and (4) yields the area distribution for the fragments of the fault plates [12]

$$p(\sigma) d\sigma = \left[1 - \frac{(1-q)}{(2-q)} (\sigma - \sigma_q) \right]^{1/(1-q)} d\sigma. \tag{7}$$

Under the assumption that the released relative energy, E, scales with the linear dimension, ρ, as $\sim \rho^3$, where ρ^3 is the volume size of a fragment, and since the surface size of a fragment scales as $\sim \rho^2$, the relation between the size of the fragments and the earthquake energy becomes

$$\sigma - \sigma_q = \left(\frac{E}{\alpha} \right)^{2/3}, \tag{8}$$

according to the scaling of the seismic moment with the rupture length [13], where α is the proportionality constant between E and ρ^3.

2.2. Cumulative Distribution of Earthquakes

The energy distribution function of earthquakes is obtained by replacing relation (8) into Equation (7) to be [12]

$$p(E) dE = \frac{C_1 E^{-1/3} dE}{\left[1 + C_2 E^{2/3} \right]^{1/(q-1)}}, \tag{9}$$

where $C_1 = 2/(3\alpha^{2/3})$ and $C_2 = (q-1)/[(2-q)\alpha^{2/3}]$. If $n(E)$ is the number of earthquakes of energy E and N_t denotes the total number of earthquakes, then the probability of the energy is given by the expression $p(E) = n(E)/N_t$. Integration of the energy distribution function (9) from E_{th} to ∞, where E_{th} is a threshold energy, and using the relation $m = (1/3) \ln E$ [37], where m is the earthquake magnitude, yields the cumulative number of earthquakes with magnitudes greater than a threshold value M, namely $N_{>M}$, in a seismic region [12]

$$\ln N_{>M} = \ln N_t + \ln \left[1 - \left(\frac{q-1}{q-2} \right) \frac{10^{2M}}{\alpha^{2/3}} \right]^{(q-2)/(q-1)}. \tag{10}$$

 doi:10.20944/preprints202405.0076.v1

It must be emphasized that the q-index in Equation (10) is related to the earthquake energy distribution (9). Equation (10) incorporates the principles of non-extensive thermodynamics into the distribution of earthquakes as a function of the magnitude and represents a widely used form of the non-extensive modification of the GR law based on the Tsallis entropy. If the same algebraic steps leading to Equation (10) are applied based on the classical BG statistics, the following frequency-magnitude is obtained

$$\ln N_{>M} = A - 10^{2M} B, \tag{11}$$

where A and B are data-adjustable parameters. In general, Equation (11) works correctly only for low seismicity, i.e., for earthquakes with magnitudes $\lesssim M_c$. In Equation (10) the entropic index q takes values in the interval $[1, 2]$, while the constant α can vary between 10^{-3} and 10^{11}. In particular, the q-index is a measure of the length scale of the spatial interactions. A q-value close to unity is indicative of short-range correlations, while higher values are indicative of long-term interactions and therefore more instability. In terms of the fragment-asperity interaction model, high values of q are indicative of fault planes in relative motion and, as a result, of the fact that more seismic events are expected [11].

3. Tectonic Setting

As was pointed out before, Mexico is a seismically-active region because its west coastline lies on the eastern rim of the Ring of Fire, where several tectonic plates interact. It is well documented that its seismicity is caused by different tectonic regimes namely, the dispersion zone in the Gulf of Baja California and two subduction processes caused by the Rivera and Cocos plates, which are subducting beneath the continental edge of the North American plate. Several studies have been conducted to investigate the Cocos subduction zone, motivated primarily by the dangerous earthquakes that took place there. In particular, complete studies of the Mexican subduction regions that take into account the geometry of the Rivera and Cocos plates can be found in Refs. [25,28,30].

The Gulf of California Rift is part of the East Pacific Rise. It is a spreading boundary where two tectonic plates are moving away from each other, leading to the formation of a new oceanic crust. It is also the southern terminus of the San Andreas Fault [38]. The abundance of neotectonic problems posed by the juxtaposition of the tectonic plates in Mexico, has forced the use of the Global Positioning System (GPS) technology, which was initially limited to some areas of the Pacific coast and mainly to the Baja California region. A number of authors [39–44] have investigated these neotectonic problems, finding that the city of La Paz (Capital of Baja California) is moving southeast relative to the Pacific plate, which is consistent with the hypothesis that the Baja California Peninsula is not completely attached to the Pacific plate. The Baja California Seismic Network (NARS-Baja) stations provided a new dataset to determine some lithospheric properties on a regional scale. These seismicity catalogues have greatly assisted tectonic studies in the Gulf of Baja California by locating active structures [45].

The Rivera microplate is located just south of the Baja California Peninsula. It is bounded to the northwest by the East Pacific Rise, to the southwest by the Rivera Transform Fault, to the southeast by a deformation zone and to the northeast by the Middle America Trench and another deformation zone, where it is found an important geological feature, the Rivera Triple Junction located at the southern end of the Baja California Peninsula. It is also described as an R-R-R (ridge-ridge-ridge) type junction, which lies along the segment of the East Pacific Rise which runs between the Rivera Transform Fault and the Tamayo Fault, although the third axis of the junction is not clearly defined. Suhardja et al. [46] investigated the subduction of the Rivera and Cocos plates in the Southwestern Mexico. Their project MARS (MApping the Rivera Subduction zone) consisted of an array of 50 temporary seismometer stations to perform the receiver function analysis. They found that the crustal thickness varies from 20 km near the coast to 42 km in the continental interior. The Rivera plate has a dip steeper than the Cocos plate along the coast and it is about 10 km deeper than was previously estimated by Pardo and Suarez [28]. The number of seismic imaging studies of the Mexican subduction zone has increased considerably in this century, unravelling the complex interaction of the tectonic plates. The southern part of the Mexican Volcanic Belt shows velocities around 0–4 mm yr^{-1} for its present slip. The

 doi:10.20944/preprints202405.0076.v1

high-resolution image obtained by the analysis of the MASE (MesoAmerican Subduction Experiment) seismic data showed that the flat slap is so shallow and stays this way nearly horizontal for 250 km, lying flat against the continental crust. The Mexican subduction zones could not only be affected by unusual thicknesses of the incoming oceanic crust, but also by atypical forearc dynamics.

Kazachkina et al. [43] revealed an active shear zone parallel to the Middle America Trench about 650 km long, by using continuous GPS records gathered over a time span of more than a decade in the Guerrero region. This left-lateral shear zone delimits a wide forearc sliver that moves over the subducting Cocos plate at a rate of 3–6 mm yr^{-1} with respect to the North American plate [47]. The long-term effects of this sliver on the subduction dynamics for the unusually shallow Mexican flat slab are still a matter of research. The subduction in southern Mexico can be approximated by a subhorizontal slab (the Flat slab) bounded at its edge by the steep subduction geometry of the Cocos plate beneath the Caribbean plate to the east and of the Rivera plate beneath the North American lithosphere to the west. Subduction zones are prone to generate strong earthquakes, as is indeed the case of the Oaxaca and Chiapas regions, which have experienced a few strong events over the years of magnitude greater than M8 [19].

On the other hand, Carciumaru et al. [48] have recently identified two slab tearings, one on the Michoacán–Guerrero border and the other in Oaxaca, near the Tehuantepec fracture Transform/Ridge. The slab tearing on the Michoacán–Guerrero border constitutes an important change in the subducting slab, while the one near the Tehuantepec fracture Transform/Ridge marks the inflection point of the trench that slightly changes its trend to the southeast of the Cocos plate convergence rate. However, the slides on both sides of the Tehuantepec Ridge are different (i.e., 6.43 and 7.2 cm yr^{-1}) [49]. Figure 1 shows a tectonic map of Mexico, where the seismic zones along the west Mexican coastline are highlighted with different colors. The location of the East Pacific Rise is marked by broken solid lines and fracture zones are marked by dashed lines. The subduction regime of Oaxaca and Chiapas is dominated by the Tehuantepec Transform/Ridge. The enhanced seismic tomography performed by Calò [49] has shown that this fracture is responsible for the vertical propagating tear that controls the magmatism of the El Chichón volcano [50,51] and has also identified the presence of lateral bending, windows, tears and incipient fragmentation in the first 200-250 km of the subducted plate.

As shown in Figure 1, in terms of its seismicity the southern part of Mexico can be divided into five main regions [19]: (1) the Jalisco region to the west, where the Rivera plate subducts at a steep angle, (2) the Michoacán region, where the dip angle of the Cocos plate decreases gradually in the southeast direction, (3) the Guerrero zone bounded by the Orozco and O'Gorman fractures, (4) the northern Oaxaca region, where the subducted slab is nearly subhorizontal and underplates the upper continental plate for $\sim$ 250 km, and (5) the southern Oaxaca and Chiapas regions bounded by the Clipperton fracture, while the Tehuantepec Ridge, which is a linear undersea ridge, extends from the eastern end of the Clipperton fracture into the Chiapas region, where the dip of the subduction increases gradually to a steeper subduction of the Central America Trench. In particular, the Tehuantepec Ridge is one prominent structure of the Cocos plate and its tectonic evolution has not been investigated in depth yet [52]. The seismicity in the northern part of the Mexican coastline is characterized by active structures in the Gulf of Baja California, which extends about 1300 km from the fast-spreading mid-ocean ridge system of the East Pacific Rise to the San Andreas Transform Fault zone in southern California. In particular, crustal deformation is active over the full length of the Gulf, ranging from classic ridge-transform structures in the south to diffuse deformation in the north [45,53].

 doi:10.20944/preprints202405.0076.v1

Figure 1. Tectonic map of Mexico. The seismic regions along the west coastline of Mexico are highlighted with different colors. The locations of the East Pacific Rise (broken solid lines) and the fracture zones (dashed lines), including the Tehuantepec Ridge are shown. The pattern brush stroke of filled triangles along the southwestern coast represents the subduction zones, with the triangles pointing in the direction of the subduction.

4. Earthquake Data and Analysis Procedure

In this work we use the corrected Mexican seismic catalogue provided by the National Seismic Service (DOI: http://www.ssn.unam.mx). The investigated period spans from January 1, 2000 to October 13, 2023. The spatial distribution of earthquakes in each of the six studied regions in Figure 1 is displayed in Figure 2. The symbols (filled dots) in each region mark the actual location of the epicenters. The spatial distribution of earthquake epicenters over each region was calculated using data from the corrected Mexican seismic catalogue with the aid of the ZMAP software for the analysis of seismic patterns. Darkest zones with the highest concentration of symbols (epicenters) are indicative of sustained seismic activity. Starting from the second column, Table 1 lists the minimum magnitude, M_{min}, the maximum magnitude, M_{max}, the number of recorded events and the magnitude of completeness, M_{c}, for each investigated region.

Table 1. Seismic activity along the west coastline of Mexico.

Region	M_{min}	M_{max}	**Number of earthquakes**	M_{c}
Baja California	1.4	6.8	9579	3.70
Nayarit-Jalisco	2.3	5.9	3774	3.30
Colima-Michoacán	1.9	7.7	20229	3.45
Guerrero	1.9	7.4	33080	3.65
Oaxaca	1.2	7.5	59803	3.46
Chiapas	1.6	8.2	67008	3.76

 doi:10.20944/preprints202405.0076.v1

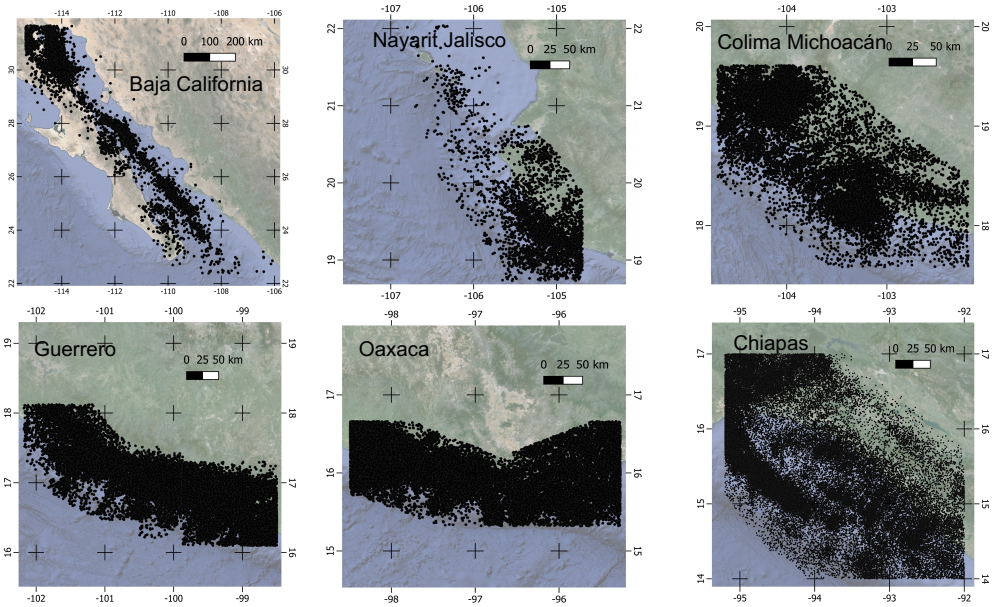

Figure 2. Spatial distribution of recorded earthquakes in the six regions investigated along the west coastline of Mexico. The symbols mark the location of the earthquake epicenters.

The Oaxaca and Chiapas regions display the largest numbers of earthquakes, while the Jalisco region has the lowest activity. The minimum magnitude varies from region to region in the interval between 1.2 (Oaxaca) and 2.3 (Jalisco). During the period investigated, the strongest earthquakes occurred in Chiapas with a magnitude of 8.2 and Michoacán with a magnitude of 7.7. With the exception of Baja California and Jalisco, all regions have experienced earthquakes with magnitudes $M > 7$. The magnitudes of completeness in the last column of Table 1 was calculated from the recorded data using the method of maximum likelihood estimation (MLE).

The data are first analyzed in terms of the classical GR law

$$\log N_{>M} = a - bM, \tag{12}$$

where the parameter a quantifies the seismicity rate of a region and b is the slope of the cumulative distribution, which is close to unity for tectonic earthquakes. This log-linear dependence of the number of earthquakes of magnitudes greater than M on the value of M fails for low and large magnitudes where the dependence deviates from linear. A non-extensive description of the catalogue data is here obtained using the normalized cumulative distribution, $N_{>M}/N_t$, given by Equation (10). For each region the value of the non-extensive parameters q and α are estimated by fitting the observed distribution with the non-extensive model of Equation (10). This was done by means of a minimization procedure using two different algorithms, namely the differential genetic evolution (DGE) [54] and the Broyden-Fletcher-Goldfarb-Shanno (BFGS) optimization algorithm [55].

5. Results

5.1. The Gutenberg-Richter (GR) Law

The classical GR law (12) has played an important historical role in seismology because it was long used to characterize local seismicity and estimate magnitudes of completeness. However, its graphical representations for different catalogues show that it cannot reproduce the correct dependence for the smallest magnitudes. It also fails to describe the energy distribution for large magnitudes. In other words, the linear fitting of the GR law cannot account for magnitudes lower than M_c and in general is not representative of extreme seismic events. Therefore, when plotting the frequency-magnitude

 doi:10.20944/preprints202405.0076.v1

relation its reliability is limited to a range of intermediate magnitudes for which the linear fitting matches the observed data.

Figure 3 depicts the GR law for the six regions examined. In each plot the red line shows how well the linear fitting of the GR law reproduces the catalogue data. In all cases, the GR relation is satisfied for magnitudes $> M_c$ and smaller than about 5. The worst case corresponds to the Oaxaca catalogue where magnitudes larger than ~ 4 does not fit the GR law. To the left of the cumulative distribution the frequency distribution of earthquakes as a function of the magnitude is also depicted for each investigated region (empty squares). In all cases the distributions peak close to the magnitude of completeness, implying that in all regions earthquakes with magnitudes $3.3 \lesssim M \lesssim 3.76$ are much more frequent, while stronger events are towards the right tail of the distribution. The values of the parameters a and b in Equation (12) are sensitive to whether or not the cumulative distribution is normalized to the number of earthquakes. Table 2 displays the values of a and b for both cases.

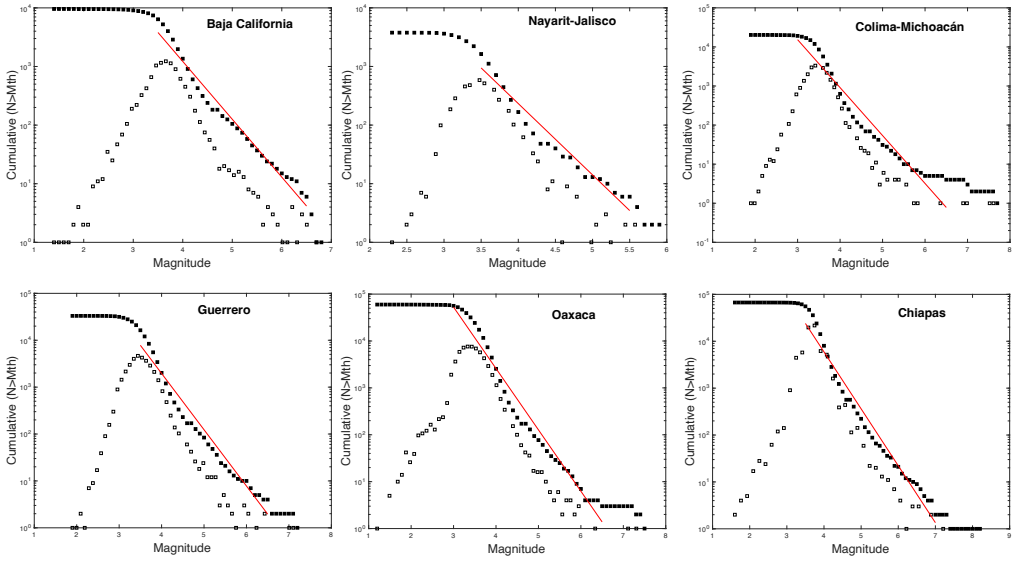

Figure 3. GR law (red line) fitted to the earthquake sub-catalogue for each of the six regions investigated (filled squares). For each region the frequency distribution of earthquakes as a function of the magnitude is depicted to the left of the cumulative distribution (empty squares).

Table 2. GR-law parameters a and b for the six regions investigated.

Region	a **for** $N_{>M}$ **(non-normalized)**	b **for** $N_{>M}$ **(non-normalized)**	a **for** $N_{>M}/N_t$ **(normalized)**	b **for** $N_{>M}/N_t$ **(normalized)**
Baja California	7.010	−0.991	3.236	−1.031
Nayarit-Jalisco	6.814	−1.135	4.435	−1.416
Colima-Michoacán	7.518	−1.148	5.480	−1.743
Guerrero	8.280	−1.243	4.132	−1.345
Oaxaca	8.634	−1.327	4.925	−1.574
Chiapas	9.266	−1.359	4.006	−1.273

When the GR law is not normalized with respect to the total number of earthquakes per region, the b-values are closer to unity than when they are normalized. In general, values of the slope close to unity mean that these regions are all seismically active. The normalized a-values are all greater than 4 with the exception of the Baja California region where $a \approx 3.24$. When $N_{>M}$ is not normalized the a-values are higher than the normalized ones by factors of about 2.

 doi:10.20944/preprints202405.0076.v1

5.2. Non-Extensive Analysis

For each region the value of the non-extensive parameters are estimated by fitting the observed distribution with the non-extensive model of Equation (10). The best fitting is obtained when the square-2 norm attains either a minimum value or reaches a fixed value by using two consecutive procedures. First, the Monte Carlo method was applied to evaluate Equation (10) in the intervals reported by Valverde-Esparza et al. [19], i.e., $1 < q < 2$ and $\alpha \in (10^{-3}, 10^{11})$. The initial value of the entropic index, q_0, is set equal to 1.5, while α_0 is chosen randomly from a million values between 10^{-3} and 10^{11} so that optimal intervals around these initial values are defined to be $q_0 \pm 0.2$ and $\alpha_0 \pm 10^{-3}$ and a couple of initial values (q_0, α_0) is then proposed. The second procedure consists of using the selected couple of values (q_0, α_0) as the initial guess for the DGE and BFGS algorithms to obtain the values of q and α. A common drawback of these methodologies is that the optimal initial values q_0 and α_0 leading to a minimum error are unknown and therefore they must be varied by trial and error until a satisfactory error level is found. The second, third, fourth and fifth columns of Table 3 list the optimal initial values of q_0 and α_0 for which a minimum error along with stable values of q and α were obtained.

Figure 4 shows the computed cumulative distribution of events for the Baja California and Jalisco regions. The solid curves represent the best fit model functions. The plots on the left side correspond to the best fit to the empirical data as obtained with the DGE method, while those on the right side are the fits obtained using the BFGS method. The fourth and fifth columns of Table 3 list the values of q and α from the DGE fitting, while those in the sixth and seventh columns list those from the BFGS fitting. Both methods yield the same values of α for both regions, i.e., $\alpha \approx 6.88 \times 10^{10}$ (Baja California) and $\alpha \approx 1.98 \times 10^{10}$ (Jalisco). Conversely, the q-values are more sensitive to the choice of the optimization method. For example the DGE method yields $q = 1.60$ (Baja California) and 1.56 (Jalisco), while the BFGS method produces slightly different values (i.e., $q = 1.55$ for the Baja California region and $q = 1.57$ for the Jalisco region).

 doi:10.20944/preprints202405.0076.v1

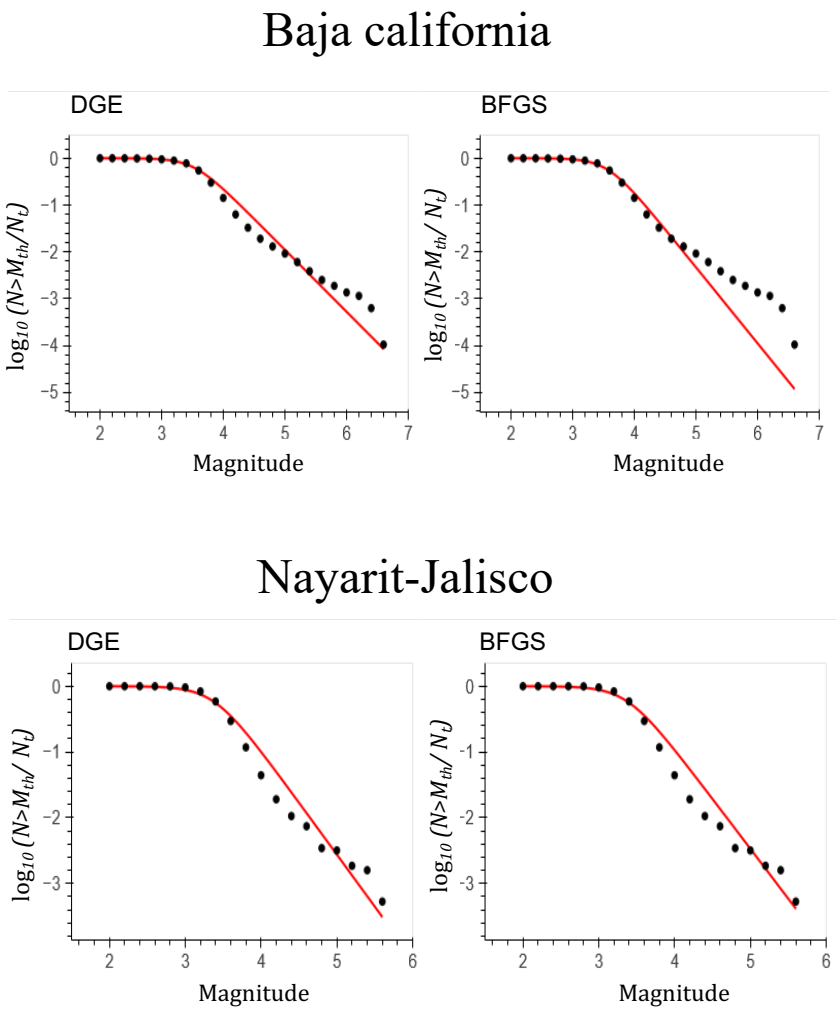

Figure 4. Normalized cumulative distribution of earthquakes for the seismicity monitored in the Baja California (upper plots) and Jalisco (lower plots) regions (filled dots). The red solid curves correspond to the fittings based on Equation (10). In each case the left and right plots depict the fitting as obtained using the DGE and BFGS method, respectively.

Table 3. Non-extensive Tsallis' entropic parameters for the six regions investigated.

Region	q_0 **(DGE)**	α_0 **(DGE)**	q **(DGE)**	α **(DGE)**	q **(BFGS)**	α **(BFGS)**
Baja California	1.50	6.87(10)	1.60	6.878(10)	1.55	6.878(10)
Nayarit-Jalisco	1.56	1.97(10)	1.56	1.978(10)	1.57	1.978(10)
Colima-Michoacán	1.58	1.50(10)	1.59	1.559(10)	1.60	1.559(10)
Guerrero	1.50	8.40(10)	1.54	5.432(10)	1.55	5.432(10)
Oaxaca	1.59	2.70(10)	1.53	2.746(10)	1.61	2.746(10)
Chiapas	1.60	2.13(11)	1.58	2.134(11)	1.59	2.134(11)
Oaxaca (part 1)	1.60	8.90(9)	1.50	8.913(9)	1.61	8.913(9)
Oaxaca (part 2)	1.60	8.00(9)	1.59	8.000(8)	1.61	8.913(9)

 doi:10.20944/preprints202405.0076.v1

As an example, the error calculated as the difference between the computed and cumulative value as a function of q_0 and α_0 is displayed in Figure 5 for the case of Baja California when the iteration was performed using the BFGS method. This plot exemplifies the procedure followed to obtain the minimum error. Similar plots were obtained for all other regions. The minimum error is achieved when $q_0 = 1.50$ and $\alpha_0 = 6.87 \times 10^{10}$. For this case the value of the error is stable for $\alpha_0 > 10^{10}$. On the other hand, Figure 6 shows the best fits obtained for the Michoacán and Guerrero regions using the DGE and BFGS methods. The DGE analysis yields q-values of 1.59 (Mochoacán) and 1.54 (Guerrero), while the BFGS analysis results in slightly higher values, i.e., 1.60 (Michoacán) and 1.55 (Guerrero). These values are comparable to the ones obtained for the Baja California and Jalisco regions, which according to Table 1 have a much lower incidence of events compared to Michoacán and Guerrero. Therefore, this suggests that all these four regions are equally unstable independently of the historical record of earthquakes.

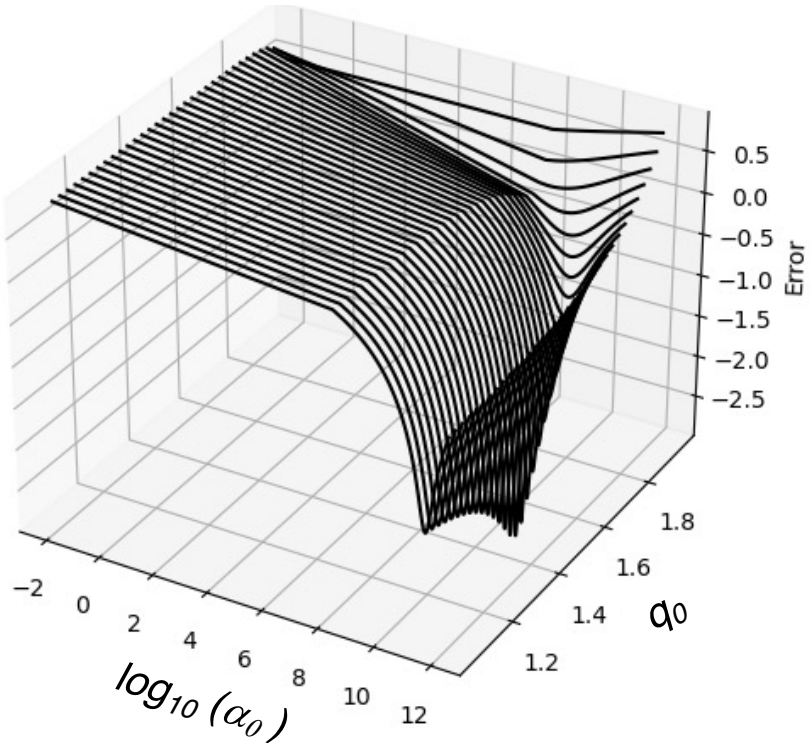

Figure 5. Runs performed by varying the initial entropic parameters q_0 and α_0 to determine the optimal guess leading to the minimum error. The figure corresponds to the case of the Baja California region using the BFGS method.

Preprints.org (www.preprints.org) | NOT PEER-REVIEWED | Posted: 1 May 2024 doi:10.20944/preprints202405.0076.v1

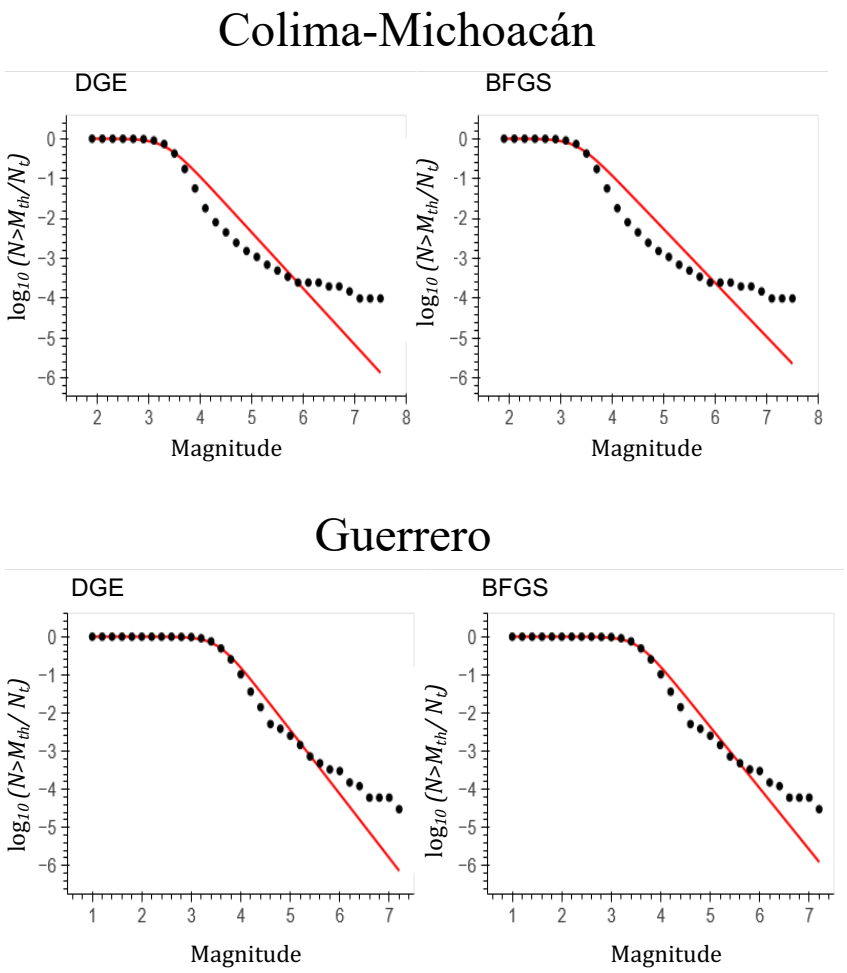

Figure 6. Normalized cumulative distribution of earthquakes for the seismicity monitored in the Michoacán (upper plots) and Guerrero (lower plots) regions (filled dots). The red solid curves correspond to the fittings based on Equation (10). In each case the left and right plots depict the fitting as obtained using the DGE and BFGS method, respectively.

Finally, Figure 7 shows the normalized cumulative distribution function for the Oaxaca and Chiapas regions. These two regions have the largest numbers of recorded earthquakes (see Table 1). However, their estimated entropic indices are $q = 1.53$ (Oaxaca) and $q = 1.58$ (Chiapas) when the analysis was performed using the DGE method. Again a much higher value of $q(= 1.61)$ was obtained for the Oaxaca region with the BFGS method, while only a slightly higher value ($q = 1.59$) was estimated for the Chiapas region. The results show that the distribution of recorded events can be well described by the generalized GR law given by Equation (10), especially for low magnitudes with q entropic indices between 1.53 and 1.60 when using the DGE method and between 1.55 and 1.61 when using the BFGS method. A comparison between both methods (Figures 4, 6 and 7) shows that BFGS performs slightly better than DGE. However, for the Baja California region DGE appears to perform better than BFGS since the latter deviates substantially from the observed data for $M > 5$ compared to the former method.

 doi:10.20944/preprints202405.0076.v1

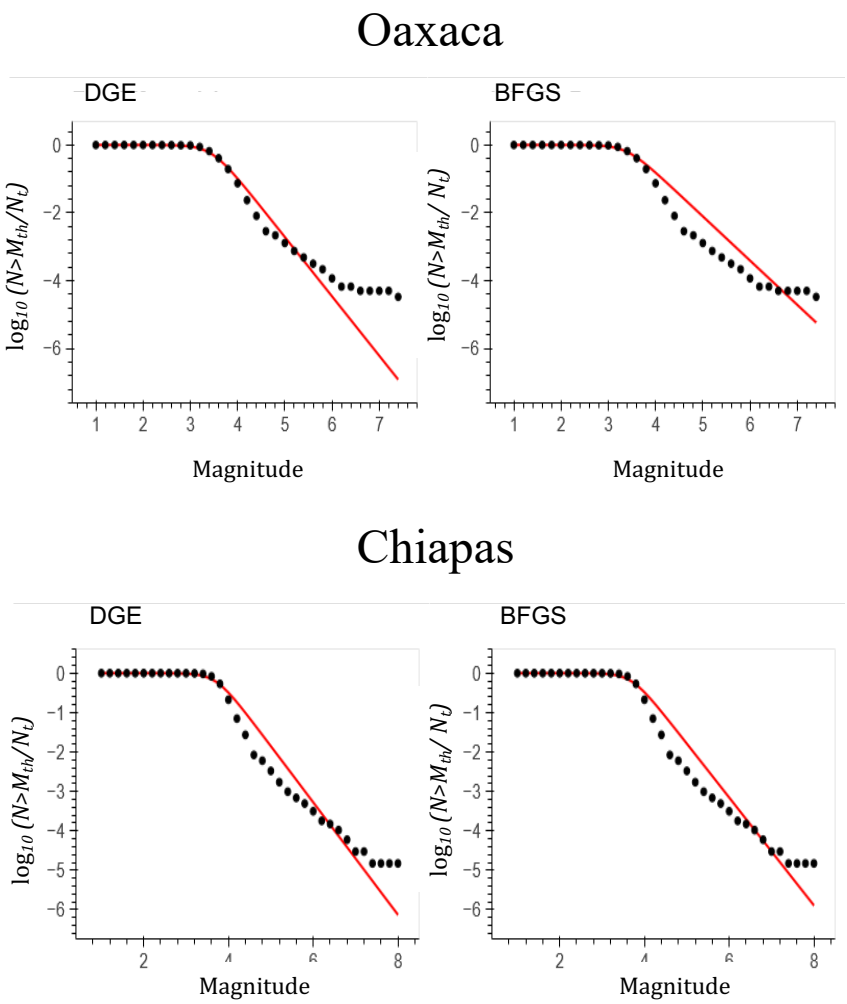

Figure 7. Normalized cumulative distribution of earthquakes for the seismicity monitored in the Oaxaca (upper plots) and Chiapas (lower plots) regions (filled dots). The red solid curves correspond to the fittings based on Equation (10). In each case the left and right plots depict the fitting as obtained using the DGE and BFGS method, respectively.

From the analysis of the frequency-magnitude distributions of all six regions, it is clear that the fragment-asperity model describes the seismic behavior of the western Mexican coastline fairly well, perhaps except at the largest magnitudes towards the lower end of the distributions. This feature is more prominent for the Baja California region (Figure 4). In other words, the entropic index q describes the complexity of the tectonic system along the Pacific coast of Mexico with values between 1.50 and 1.60, supporting sub-additivity of the frequency-magnitude distribution of earthquakes. A previous non-extensive analysis of seismicity in Mexico, spanning the period from 1988 to 2000, have yielded values of the entropic index in the interval $1.663 \lesssim q \lesssim 1.702$ for the southern Mexican seismicity, comprising the regions of Jalisco, Michoacán, Guerrero and Oaxaca [19]. These values are, however, larger than those reported by the present analysis. A possible cause of this difference can be attributed to the use of improved seismic recording equipment during the last decade, which is more sensitive to the detection of low-magnitude events than older instrumentation, and to the increasing number of seismic stations. Increasing the number of recorded earthquakes of low magnitude will contribute to lower the estimated values of the entropic index q.

A close inspection of the two upper plots of Figure 7 for the Oaxaca region reveals that the observed data for magnitudes $> M_c$ are characterized by at least three different slopes for low ($M_c \lesssim M \lesssim 4.5$), intermediate ($4.5 \lesssim M \lesssim 6.4$) and large ($M \gtrsim 6.5$) magnitudes. This means that

 doi:10.20944/preprints202405.0076.v1

it is not possible to fit a unique curve for the whole range of magnitudes in the Oaxaca region as was first reported by Valverde-Esparza et al. [19]. In particular, the crossover at a magnitude of about 4.5 is indicative of the Oaxaca region being characterized by two different subduction processes since this region comprises the earthquakes that took place in the zones between the Tehuantepec Transform/Ridge and the Clipperton fracture (Oaxaca, part 2) and the zones between the Clipperton and O'Gorman fractures (Oaxaca, part 1). Figure 8 shows the normalized cumulative distribution of events for both sub-regions as obtained with the DGE (left plots) and BFGS (right plots) optimization methods. These fits provided values of $q = 1.50$ with the DGE method and $q = 1.61$ with BFGS method for Oaxaca, part 1 and values of $q = 1.59$ with the DGE method and $q = 1.61$ with the BFGS method for Oaxaca, part 2 (see Table 3). It is clear that the q-values for the Oaxaca, part 2 sub-region are closer to those for the Chiapas region, while those derived for the Oaxaca, part 1 sub-region are closer to those corresponding to the Guerrero region. This latter statement is at least valid for the DGE values. We note that the same is not necessarily true for the BFGS values where $q = 1.61$ for the complete and the two sections of the Oaxaca catalogue.

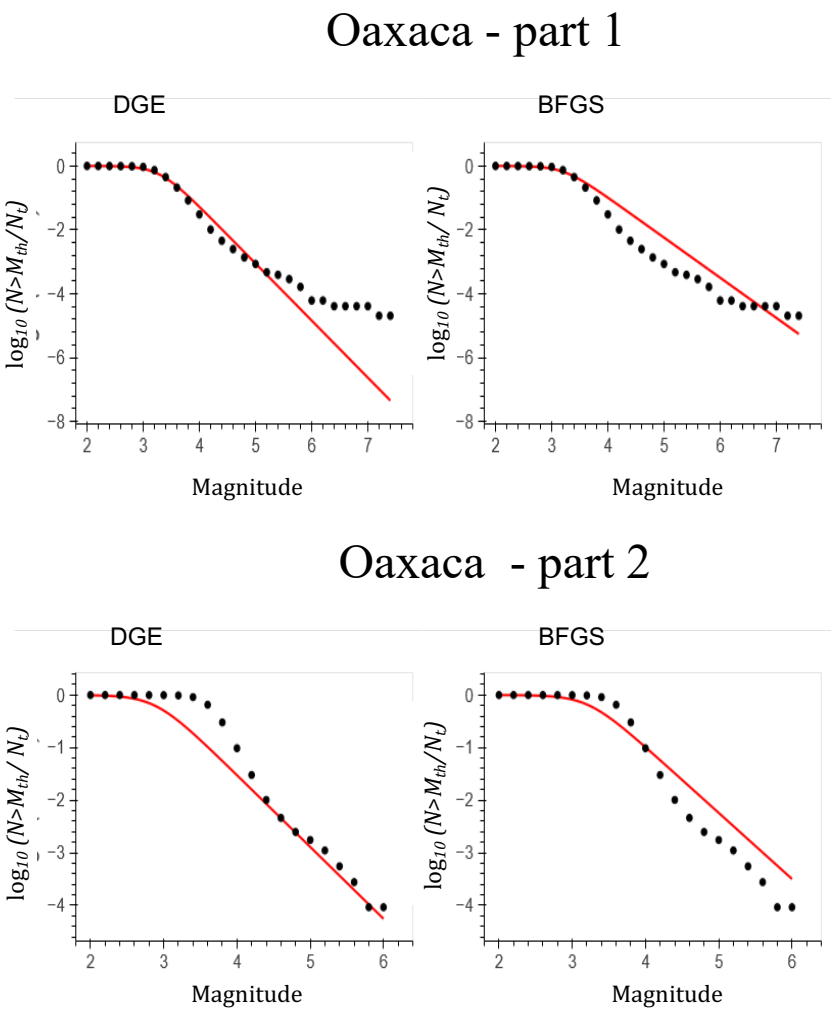

Figure 8. Normalized cumulative distribution of earthquakes for the seismicity monitored in the Oaxaca sub-regions, part 1 (upper plots) and part 2 (lower plots). The filled dots corresponds to the monitored catalogue data, while the red solid curves correspond to the fittings based on Equation (10). In each case the left and right plots depict the fitting as obtained using the DGE and BFGS method, respectively.

 doi:10.20944/preprints202405.0076.v1

6. Conclusions

A seismic analysis of magnitude catalogues from 2000 to 2023 of the Mexican South Pacific was performed by means of the NESM approach based on the Tsallis formalism. We analyzed six regions along the west coastline of Mexico, namely Baja California, Jalisco-Nayarit, Colima-Michoacán, Guerrero, Oaxaca and Chiapas, which are characterized by different tectonic regimes. The seismicity of the Gulf of Baja California (Cortes Sea) is caused by the dispersion zone which is a continuation of the San Andreas Fault. In contrast, the seismic activity in the Jalisco-Nayarit and Colima-Michoacan regions is mainly due to the subduction process of the Rivera plate, while the seismicity of the Guerrero, Oaxaca and Chiapas regions is mainly caused by the subduction of the Cocos plate. In both cases the plates are subducting beneath the continental edge of the North American plate. The relevant conclusions are summarized as follows:

1. According to the Gutenberg-Richter (GR) law all six regions have magnitudes of completeness in the range between 3.30 and 3.76, implying that along the Pacific coast of Mexico earthquakes with magnitudes in this range are more frequent.
2. The Oaxaca and Chiapas regions share the largest number of earthquakes, while the regions of Jalisco and Baja California have the lowest activity.
3. The GR-law parameters a and b are sensitive to whether or not the cumulative distribution is normalized to the number of earthquakes. In particular, the normalized b-parameter is close to unity for all six regions, meaning that they are all seismically active.
4. A non-extensive model fitting with the observed distributions of earthquakes was obtained using two different optimization methods, namely the differential genetic evolution (DGE) and the Broyden-Fletcher-Goldfarb-Shanno (BFGS) algorithm. The entropic index, q, and the parameter, α, as derived from both methods show little differences, which for q are less than about 0.05 for all cases studied.
5. The α-values ranged between 1.559×10^{10} (for the Colima-Michoacán region) and a maximum value of 2.134×10^{11} (for the Chiapas region).
6. The whole range of magnitudes recorded for the Oaxaca region cannot be fitted by a unique curve since for magnitudes close to 5 the slope of the normalized cumulative magnitude distribution changes, implying a clear crossover for this region. When both sub-regions are analyzed separately both optimization methods predict lower values of α.
7. A value of q close to unity is indicative of short-range correlations, while higher values are indicative of long-term interactions and, therefore of more instability. In terms of the fragment-asperity interaction model, values of $q > 1$ are indicative of fault planes in relative motion, implying that more seismic events are expected. All six regions display values of q greater than 1.52, suggesting instability and long-term correlations. In particular, the regions of Baja California, Colima-Michoacán and Chiapas had the largest values of q between 1.58 and 1.60.
8. In comparison with a previous similar analysis spanning the period from 1988 to 2010, updated estimates of q were obtained to be from 1.70 to 1.56-1.57 for Jalisco, from 1.68 to 1.59-1.60 for Michoacán, from 1.64 to 1.54-1.55 for Guerrero and from 1.66 to 1.53-1.61 for Oaxaca. The predicted lower values of q are a consequence of the use of new instrumentation, which is more sensitive to the detection of low-magnitude earthquakes.

Author Contributions: Conceptualization, E.L.F.-M. and A.R.-R.; methodology, E.L.F.-M., A.R.-R. and L.DiG.S.; formal analysis, E.L.F.-M. and A.R.-R.; investigation, E.L.F.-M.; data curation, E.L.F.-M., A.R.-R. and L.DiG.S.; writing—original draft preparation, L.DiG.S.; writing—review and editing, L.DiG.S., A.R.-R. and E.L.F.-M.; supervision, E.L.F.-M.; funding acquisition, E.L.F.-M., A.R.-R. and L.DiG.S. All authors have read and agreed to the published version of the manuscript.

Funding: This research received no external funding.

Data Availability Statement: The research data employed in this paper are available upon reasonable request to the corresponding author.

Acknowledgments: E.L.F-M. is grateful to the Instituto de Geofísica of the Universidad Nacional Autónoma de México for financial and technical support, while A.R.-R. and L.DiG.S. acknowledge the Departamento de

 doi:10.20944/preprints202405.0076.v1

Ciencias Básicas of the Universidad Autónoma Metropolitana, Azcapotzalco Campus for financial support. We thank Raúl Velázquez for helping us in the optimization calculations.

Conflicts of Interest: The authors declare no conflict of interest.

References

1. Tsallis, C. What should a statistical mechanics satisfy to reflect nature?. *Phys. D* **2004**, *193*, 3–34.
2. Tsallis, C. Nonadditive entropy and nonextensive statistical mechanics – An overview after 20 years. *Braz. J. Phys.* **2009**, *39*, 337–356.
3. Tsallis, C.; Tirnakli, U. Nonadditive entropy and nonextensive statistical mechanics – Some central concepts and recent applications. *J. Phys. Conf. Ser.* **2010**, *201*, 012001.
4. Tsallis, C. Possible generalization of Boltzmann-Gibbs statistics. *J. Stat. Phys.* **1988**, *52*, 479–487.
5. Abe, S.; Okamoto, Y. *Nonextensive Statistical Mechanics and Its Applications*; Springer-Verlag: Heidelberg, Germany, 2001.
6. Tsallis, C. *Introduction to Nonextensive Statistical Mechanics: Approaching a Complex World*, Springer: Berlin, Germany, 2009.
7. Tsallis, C. The nonadditive entropy S_q and its applications in physics and elsewhere: Some remarks. *Entropy* **2011**, *13*, 1765–1804.
8. Abe, S.; Suzuki, N. Law for the distance between successive earthquakes. *J. Geophys. Res.* **2003**, *108*(B2), 2113.
9. Papadakis, G.; Vallianatos, F.; Sammonds, P. Evidence of nonextensive statistical physics behavior of the Hellenic subduction zone sismicity. *Tectonophys.* **2013**, *608*, 1037–1048.
10. Vallianatos, F.; Sammonds, P. Evidence of nonextensive statistical physics of the lithospheric instability approaching the 2004 Sumatran-Andaman and 2011 Honshu mega-earthquakes. *Tectonophys. 2004*, *590*, 52–58.
11. Sotolongo-Costa, O.; Posadas, A. Fragment-asperity interaction model for earthquakes. *Phys. Rev. Lett.* **2004**, *13*(7), 1267–1280.
12. Silva, R.; França, G. S.; Vilar, C. S.; Alcaniz, J. S. Nonextensive models for earthquakes. *Phys. Rev. E* **2006**, *73*, 026102.
13. Lay, T.; Wallace, T. C. *Modern Global Seismology*; Academic Press: New York, USA, 1995.
14. Telesca. L. Maximum likelihood estimation of the nonextensive parameters of the earthquake cumulative magnitude deistribution. *Bull. Seismol. Soc. Am.* **2012**, *102*, 886–891.
15. Darooneh, A. M.; Mehri, A. A nonextensive modification of the Gutenberg-Richter law: q-stretched exponential form. Phys. A **2010**, *389*, 509–514.
16. Telesca, L. Analysis of Italian seismicity by using a nonextensive approach. *Tectonophys.* **2010**, *494*, 155–162.
17. Telesca, L. Nonextensive analysis of seismic sequences. *Phys. A* **2010**, *389*, 1911–1914.
18. Matcharashvili, T.; Chelidze, T.; Javakhishvili, Z.; Jorjiashvili, N.; Fra Paleo, U. Non-extensive statistical analysis of seismicity in the area of Javakheti, Georgia. *Comput. Geosci.* **2011**, *37*, 1627–1632.
19. Valverde-Esparza, S. M.; Ramírez-Rojas, A.; Flores-Márquez, E. L.; Telesca, L. Non-extensivity analysis of seismicity within four subduction regions in Mexico. *Acta Geophys.* **2012**, *60*, 833–845.
20. Antonopoulos, C. G.; Michas, G.; Vallianatos, F. Evidence of q-exponential statistics in Greek seismicity. *Phys. A* **2014**, *409*, 71–77.
21. Papadakis, G.; Vallianatos, F.; Sammonds, P. A nonextensive statistical physics analysis of the 1995 Kobe, Japan earthquake. *Pure Appl. Geophys.* **2015**, 172, 1923–1931.
22. Papadakis, G.; Vallianatos, F.; Sammonds, P. Non-extensive statistical physics applied to heat flow and the earthquake frequency-magnitude distribution in Greece. *Phys. A* **2016**, *456*, 135–144.
23. Papadakis, G.; Vallianatos, F. Non-extensive statistical physics analysis of earthquake magnitude in North Aegean Trough, Greece. *Acta Geophys.* **2017**, *65*, 555–563.
24. Ohtake, M.; Matumoto, T.; Latham, G. V. Evaluation of the forecast of the 1978 Oaxaca, Southern Mexico earthquake based on a precursory seismic quiescence. In *Earthquake Prediction: An International Review*; Simpson, D. W., Richards, P. G., Eds.; Publications: Washington, USA, 1981; pp. 53–61.
25. Singh, S. K.; Rodriguez, M.; Esteva, L. Statistics of small earthquakes and frequency of occurrence of large earthquakes along the Mexican subduction zone. *Bull. Seismol. Soc. Am.* **1983**, *73*(6A), 1779–1796.

 doi:10.20944/preprints202405.0076.v1

26. Singh, S. K.; Ponce, L.; Nishenko, S. P. The great Jalisco, Mexico, earthquakes of 1932: Subduction of the Rivera plate. *Bull. Seismol. Soc. Am.* **1985**, *75*(5), 1301–1313.
27. Kostoglodov, V.; Ponce, L. Relationship between subduction and seismicity in the Mexican part of the Middle America Trench. *J. Geophys. Res.* **1994**, *99*(B1), 729–742.
28. Pardo, M.; Suarez, G. Shape of the subducted Rivera and Cocos plates in southern Mexico: Seismic and tectonic implications. *J. Geophys. Res.* **1995**, *100*(B7), 12357–12373.
29. Zúñiga, F. R.; Wiemer, S. Seismic patterns: are they always related to natural causes? *Pure Appl. Geophys.* **1999**, *155*(2-4), 713–726.
30. Iglesias, A.; Singh, S. K.; Lowry, A. R.; Santoyo, M.; Kostoglodov, V.; Larson, K. M.; Franco-Sánchez, S. I. The silent earthquake of 2002 in the Guerrero seismic gap, Mexico ($M_w = 7.6$): Inversion of slip on the plate interface and some implications. *Geof. Int.* **2004**, *43*, 309–317.
31. Song, T.-R. A.; Helmberger, D. V.; Brudzinski, M. R.; Clayton, R. W.; Davis, P.; Pérez-Campos, X.; Singh, S. K. Subducting slab ultra-slow velocity layer coincident with silent earthquakes in southern Mexico. *Science* **2009**, *324*(5926), 502–506.
32. Ramírez-Herrera, M. T.; Kostoglodov, V.; Urrutia-Fucugauchi, J. Overview of recent coastal tectonic deformation in the Mexican subduction zone. *Pure Appl. Geophys.* **2011**, *168*(8-9), 1415–1433.
33. Ramírez-Rojas, A.; Flores-Márquez, E. Order parameter analysis of seismicity of the Mexican Pacific coast. *Phys. A* **2013**, *392*, 2507–2512.
34. Ramírez-Rojas, A.; Flores-Márquez, E. L.; Sarlis, N. V.; Varotsos, P. A. The complexity measures associated with the fluctuations of the entropy in natural time before the deadly Mexico M8.2 earthquake on 7 September 2017. *Entropy* **2018**, *20*, 477.
35. Sarlis, N. V.; Skordas, E. S.; Varotsos, P. A.; Ramírez-Rojas, A.; Flores-Márquez, E. L. Natural time analysis: On the deadly Mexico M8.2 earthquake on 7 September 2017. *Phys. A* **2018**, *506*, 625–634.
36. Abe, S. Geometry of escort distributions. *Phys. Rev. E* **2003**, *68*(3), 031101.
37. Kanamori, H.; Stewart, G. S. Seismological aspects of the Guatemala earthquake of February 4, 1976. *J. Geophys. Res.* **1978**, *83*, 3427–3434.
38. Lewis, J. L.; Day, S. M.; Magistrale, H.; Castro, R. R.; Astiz, L.; Rebollar, C.; Eakins, J.; Vernon, F. L.; Brune, J, N. Crustal thickness of the peninsular ranges and gulf extensional province in the Californias. *J. Geophys. Res.* **2001**, *106*(B7), 13599–13611.
39. Hearn, T.M.; Clayton, R. W. Lateral velocity variations in southern California. I. Results for the upper crust from Pg waves. *Bull. Seismol. Soc. Am.* **1986**, *76*(2), 495–509.
40. Humphreys, E. D.; Clayton, R. W. Tomographic image of the southern California mantle. *J. Geophys. Res.* **1990**, *95*(B12), 19725–19746.
41. Márquez-Azúa, B.; DeMets, C. Crustal velocity field of Mexico from continuous GPS measurements, 1993 to June 2001: Implications for the neotectonics of Mexico. *J. Geophys. Res.* **2003**, *100*(B9), 2450.
42. Clayton, R. W.; Heaton, T. H.; Chandy, M.; Krause, R. A.; Kohler, M.; Bunn, J.; Guy, R.; Olson, M.; Faulkner, M.; Cheng, M.; Strand, L.; Chandy, R.; Obenshain, D.; Liu, A.; Aivazis, M. Community seismic network. *Annals Geophys.* **2011**, *54*(6), 738–747.
43. Kazachkina, E.; Kostoglodov, V.; Cotte, N.; Walpersdorf, A.; Ramírez-Herrera, M. T.; Gaidzik, K.; Husker, A.; Santiago, J. A. Active 650-km long fault system and Xolapa sliver in Southern Mexico. *Front. Earth Sci.* **2020**, *8*, 155.
44. Schellart, W. P. Control of subduction zone age and size on flat slab subduction. *Front. Earth Sci.* **2020**, *8*, 26.
45. Clayton, R. W.; Trampert, J.; Rebollar, C.; Ritsema, J.; Persaud, P.; Paulssen, H.; Pérez-Campos, X.; van Wettum, A.; Pérez-Vertti, A.; DiLuccio, F. The NARS-Baja seismic array in the Gulf of California rift zone. *MARGINS Newslett.* **2004**, *13*, 1–8.
46. Suhardja, S. K.; Grand, S. P.; Wilson, D.; Guzman-Speziale, M.; Gomez-Gonzalez, J. M.; Dominguez-Reyes, T.; Ni, J. Crust and subduction zone structure of Southwestern Mexico. *J. Geophys. Res.* **2003**, *120*(2), 1020–1035.
47. Manea, V. C.; Manea, M.; Chen, M., van Hunen, J.; Konrad-Schmolke, M. *Editorial: Unusual subsduction processes Font. Earth Sci.* **2020**, *8*, 607697.
48. Carciumaru, D.; Ortega, R.; Castellanos, J. C.; Huesca-Pérez, E. Crustal characteristics in the subduction zone of Mexico: Implication of the tectonostratigraphic terranes on slab tearing. *Seism. Res. Lett.* **2020**, *91*(3), 1781–1793.

 doi:10.20944/preprints202405.0076.v1

49. Calò, M. Tears, windows, and signature of transform margins on slabs. Images of the Cocos plate fragmentation beneath the Tehuantepec isthmus (Mexioc) using Enhanced Seismic Models. *Earth Planet. Sci. Lett.* **2021**, *560*, 116788.
50. de Ignacio, C.; Casteiñeiras, P.; Márquez, A.; Oyarzun, R.; Lillo, J.; López, I. El Chichón Volcano (Chiapas Volcanic Belt, Mexico) transitional Calc-Alkaline to Adakitic-like magmatism: Petrologic and tectonic implications. *Int. Geol. Rev.* **2003**, *45*(11), 1020–1028.
51. Manea, M.; Manea V. C. On the origin of the El Chichón volcano and subduction of Tehuantepec Ridge: A geodynamical perspective. *J.Volcanol. Geotherm. Res.* **2008**, *175*(4), 459–471.
52. Manea, M.; Manea, V. C.; Ferrari, L.; Kostoglodov, V. Tectonic evolution of the Tehuantepec Ridge. *Earth and Planetary Science Letters* **2005**, *238*(1-2), 64–77.
53. Di Luccio, F.; Persaud, P.; Clayton, R. W. Seismic structure beneath the Gulf of California: a contribution from group velocity measurements. *Geophysical Journal International* **2014**, *199*(3), 1861–1877.
54. Goldberg, D. E. *Genetic Algorithms in Search, Optimization and Machine Learning*, Kluwer Academic Publishers: Boston, 1989.
55. Fletcher, R. *Practical Methods of Optimization*, John Wiley & Sons: New York, 1987.